Hadronic Response and e/π Separation with the H1 Lead/Fibre Calorimeter

H1 SPACAL group

Abstract

Hadronic response and electron identification performance of the new H1 lead-scintillating fibre calorimeter are investigated in the 1 to 7 GeV energy range using data taken at the CERN Proton Synchrotron. The energy response to minimum ionizing particles and interacting pions are studied and compared to Monte Carlo simulations. The measured energy of pions interacting either in the electromagnetic or in the hadronic section is found to scale linearly with the incident energy, providing an energy resolution $\sigma/E \sim 38$ % within a depth of one interaction length and $\sigma/E \sim 29$ % for a total depth of two interaction lengths. Several electron identification estimators are studied and combined as a function of energy and impact point. The probability for pions to be misidentified as electrons of any measured energy above 1 GeV ranges from 5 % (for 2 GeV incident pions) to 0.4 % (at 7 GeV) for an electron detection efficiency of 90 %. The probability for pions of a given energy to be misidentified as electrons of the same energy falls to 0.25 % at 7 GeV.

To be submitted to NIM

H1 SPACAL Group

R.-D. Appuhn[4], C. Arndt[4], E. Barrelet[10], R. Barschke[4], U. Bassler[10], R. Buchholz[4], D. Bruncko[6], S. Chechelnitski[8] B. Claxton[14], G. Cozzika[3], J. Cvach[11], S. Dagoret-Campagne[10], W.D. Dau[15], H. Deckers[2], T. Deckers[2], F. Descamps[10], M. Dirkmann[2], J. Dowdell[14], V. Efremenko[8], E. Eisenhandler[7], A.N. Eliseev[17], J. Ferencei[5], B. Fominykh[8], U. Goerlach[4], L.A. Gorbov[17], I. Gorelov[8], L. Hajduk[13], I. Herynek[11], J. Hladký[11], M. Hütte[2], H. Hutter[2], W. Janczur[13], J. Janoth[5], L. Jönsson[16], H. Kolanoski[2], V. Korbel[4], F. Krivan[6], D. Lacour[10], F. Lamarche[9], M.P.J. Landon[7], B. Laforge[3], J.-F. Laporte[3], F. Lehner[4], R. Maraček[6], K. Meier[5], A. Meyer[4], A. Migliori[9], F. Moreau[9], G. Müller[4], P. Murín[6], V. Nagovizin[8], T.C. Nicholls[1], D. Ozerov[8], E. Perez[3], J.P. Pharabod[9], R. Pöschl[2], K.Rybicki[13], A. Rostovtsev[8], C. Royon[3], S. Schleif[5], A. Schuhmacher[2], A. Semenov[8], V. Shekelyan[8], Y. Sirois[9], P.A. Smirnov[17,c], V. Solochenko[8], J. Špalek[6], S. Spielmann[9], H. Steiner[4,f], J. Stiewe[5], V. Tchernyshov[8], S. Valkár[12], D. VanDenPlas[9], G. Villet[3], K. Wacker[2], A. Walther[2], M. Weber[4], D. Wegener[2], T. Wenk[2], J. Žáček[12], A. Zhokin[8] and K. Zuber[5],

[1] *School of Physics and Space Research, University of Birmingham, Birmingham, UK*[a]
[2] *Institut für Physik, Universität Dortmund, Dortmund, Germany*[b]
[3] *CEA, DSM/DAPNIA, CE-Saclay, Gif-sur-Yvette, France*
[4] *DESY, Hamburg, Germany*[b]
[5] *Institut für Hochenergiephysik, Universität Heidelberg, Heidelberg, Germany*[b]
[6] *Institute of Experimental Physics, Slovak Academy of Sciences, Košice, Slovak Republic*[c]
[7] *Queen Mary and Westfield College, London, UK*[a]
[8] *Institute for Theoretical and Experimental Physics, Moscow, Russia*
[9] *LPNHE, Ecole Polytechnique, IN2P3-CNRS, Palaiseau, France*
[10] *LPNHE, Universités Paris VI and VII, IN2P3-CNRS, Paris, France*
[11] *Institute of Physics, Czech Academy of Sciences, Praha, Czech Republic*[c,d]
[12] *Nuclear Center, Charles University, Praha, Czech Republic*[c,d]
[13] *Insitute for Nuclear Physics, Cracow, Poland*[e]
[14] *Electronics Division, Rutherford Appleton Laboratory, Chilton, Didcot, UK*[a]
[15] *Institut für Reine und Angewandte Kernphysik, Universität Kiel, Kiel, Germany*[b]
[16] *Physics Department, University of Lund, Sweden*[g]
[17] *Lebedev Physical Institute, Moscow, Russia*

[a] *Supported by the UK Particle Physics and Astronomy Research Council, and formerly by the UK Science and Engineering Research Council*
[b] *Supported by the Bundesministerium für Forschung und Technologie, FRG under contract numbers 6DO57I, 6HH27I, 6HD27I and 6KI17P*
[c] *Supported by the Deutsche Forschungsgemeinschaft*
[d] *Supported by GA ČR, grant no. 202/93/2423, GA AV ČR, grant no. 19095 and GA UK, grant no. 342*
[e] *Supported by the Polish State Committee for Scientific Research, grant No. 204209101*

[f] *Permanent address: Lawrence Berkeley Laboratory, University of California, Berkeley, California 94720*
[g] *Supported by the Swedish Natural Science Council*

1 Introduction

The interest in the high gluon density regime probed by deep inelastic processes at the *ep* collider HERA has led to the upgrade [1] of the region at large (relative to the incident proton direction) electron scattering angles in the H1 detector [2]. The heart of the upgrade is a new lead/scintillating fibre calorimeter, the SPACAL.

A key criterion for the optimization of its final design is the capability for separation of an electron signal from the huge hadronic background from photoproduction events. This requires $\pi^{\pm}$ rejection factors larger than 10^2 in the region below 10 GeV. The new calorimeter should moreover provide the best possible measurement of the hadronic energy flow, within the small detector depth available.

Several tests have been made at the CERN Proton Synchrotron (PS) in 1994-1995 to verify whether the calorimeter design and the associated trigger electronics fulfil the requirements for timing and energy resolution [3] as well as e/π separation. Here the final results on the e/π separation achievable with the SPACAL calorimeter are presented together with a detailed study of its response to hadrons.

Sections 2 and 3 describe respectively the experimental set-up (beam line, detectors, readout) and the collected data. Section 4 is dedicated to the detector energy response to incoming electrons and pions: the energy distributions from electrons and minimum ionizing particles (mips) are studied and compared with Monte Carlo simulations. Section 5 describes the electromagnetic and hadronic shower profiles. The e/π separation properties of the calorimeter are extensively discussed in Section 6.

2 Experimental set-up

2.1 Overview

The measurements were performed with two portions of the final electromagnetic and hadronic sections of the H1 SPACAL. The calorimeter modules were installed at the CERN PS T9 beam line [4], where electron and pion beams were used in the 1 to 7 GeV momentum range. After adjusting the beam collimators for an optimal momentum spread (~ 1 %), typical beam rates were of the order of 10^4 to 10^5 particles per 2.5 s spill, the spills being repeated every 14 s. The electron beam content was strongly energy dependent, varying from ~ 85 % at 1 GeV to ~ 10 % at 7 GeV. Particle identification was provided by two gas threshold Čerenkov counters installed upstream in the test area. An overview of the test area is shown in Fig. 1.

The beam travelled about 12 m from the end of the vacuum pipe to the front face of the electromagnetic module. The trigger was defined by the coincidence of the scintillator counters S1 (15×15 cm^2), S2 and S3 (1×2 cm^2 each). The mutually perpendicular arrangement of S2 and S3 defined an effective acceptance of 1×1 cm^2. A large veto scintillator with a circular hole of radius of 1.5 cm was used to suppress pile-up from beam halo particles by vetoing data acquisition for 1 μs each time the counter fired. The beam impact position was determined to better than 1 mm by a drift chamber placed between the trigger counters and the calorimeters [5]. Both the electromagnetic and the hadronic sections were mounted on a platform that could be moved horizontally and vertically

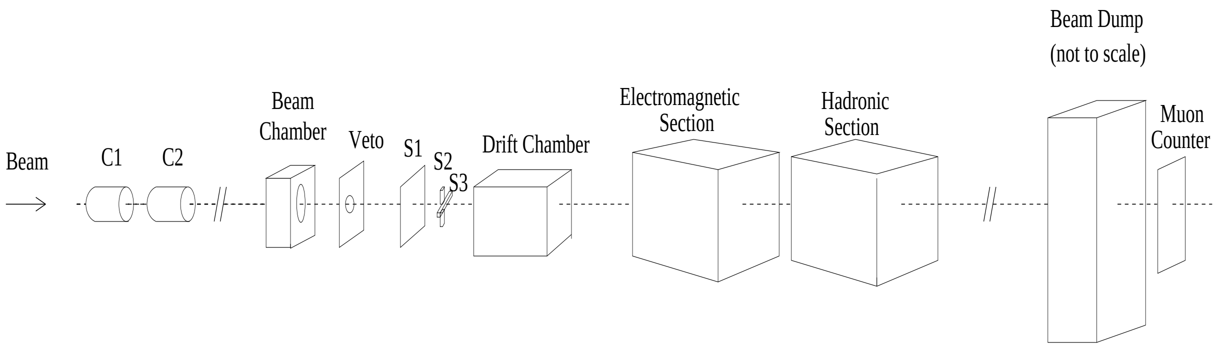

Figure 1: Layout of the test area.

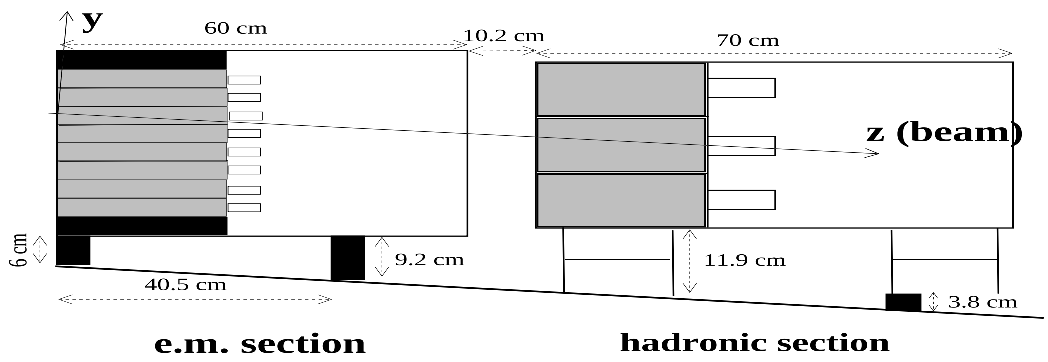

Figure 2: Alignment of the electromagnetic and hadronic sections (only the rotation around the x axis is visible here).

with respect to the beam line, with a precision better than 1 mm. Moreover, the platform could be rotated around its vertical axis so that the beam could be sent into the detector at a chosen angle with respect to the fibre axis. The accuracy of the angular movement was of the order of 2 mrad. The SPACAL electromagnetic and hadronic sections were both rotated around the x (y) axis by an angle ψ_x (ψ_y) $\sim 4.5°$. Their relative alignment (Fig. 2) was such that the beam axis would go through the center of the hadronic section when entering the middle of the electromagnetic reference cell (corresponding to cell 40 in Fig. 3: see section 3.1).

2.2 The calorimeters

2.2.1 Mechanical properties

The electromagnetic part consisted of an array of 8×8 cells, grouped in 4 supermodules of 16 cells each. The hadronic section contained 9 cells, assembled in a 3×3 array. The SPACAL mechanical structure is described in detail elsewhere [6]. Table 1 gives the main design parameters for electromagnetic and hadronic cells. The radiation and interaction length, as well as the Molière radius, were calculated according to standard prescriptions given in [7].

The optical fibres coming out from the rear end of an electromagnetic (hadronic) cell were bundled and coupled through a light mixer to a 1" (2") photomultiplier. An air gap separated the fibres from the light mixer, the latter being glued to the photomultiplier surface. Mesh dynode photomultipliers were chosen because they can operate in the high magnetic field of about 1 Tesla of H1 [8].

Parameter	Electromagnetic section	Hadronic section
Pb/fibre volume ratio	2.27/1	3.4/1
Fibre diameter (type)	d=0.5 mm (Bicron BCF-12)	d=1.0 mm (Bicron BCF-12)
Active length	25 cm	25 cm
Cell size	40.5 × 40.5 mm^2	119.3 × 119.0 mm^2
Radiation length	0.90 cm	0.84 cm
Molière radius	2.54 cm	2.46 cm
Interaction length	$\sim$ 25 cm	$\sim$ 24 cm
Photomultiplier tubes	1" (Hamamatsu R-5505)	2" (Hamamatsu R-2490-06)

Table 1: Design parameters of the H1-SPACAL cells.

2.2.2 The readout

Signals from the photomultipliers of the electromagnetic section were sent in groups of 16 to 4 analog cards located inside an analog box (ANBX). They were split into three separate paths [9]: one for the energy readout, one for the fast time-of-flight selection needed by the H1 Central Trigger logic at HERA to reject proton induced background and one for the H1 SPACAL electron trigger [10]. In the energy readout branch, the shaped signal was treated in a similar way as for the H1 Liquid Argon calorimeter [2]. The peak of the shaped pulse was sampled at the maximum for subsequent analog to digital conversion (ADC). Parallel tests of the two other paths of the electronics were performed but they are not described in this paper.

At CERN, this conversion was controlled and read out by a Digital Signal Processor (DSP) that made the data available to an OS9 acquisition system on a trigger request. The 9 signals from the hadronic section were sent to a CAMAC charge-integrating ADC. The beam counters (scintillators and Čerenkov counters) were read out by CAMAC ADCs and TDCs. Pulses from the drift chamber were also recorded by CAMAC TDCs. All these CAMAC modules were read out by the OS9 acquisition system.

3 Data sets and event selection

3.1 Beam test data

SPACAL electromagnetic cells were calibrated at the beginning of the test period with 4 GeV electrons. About 1000 electrons were sent into the center of each cell. By adjusting the photomultiplier high voltages, the gains of the 64 cells were equalized to the level of 1 %, giving a global calibration constant of 4.4 MeV per ADC count.

The gain adjustment of the hadronic cells was made at the beginning of the test period by equalizing the response to minimum ionizing particles. The final intercalibration was obtained at the end of the test with a 2 GeV electron beam after removing the electromagnetic section from the beamline. This yielded an average calibration constant of 6.2 MeV per ADC count with a systematic uncertainty of the order of 0.5%.

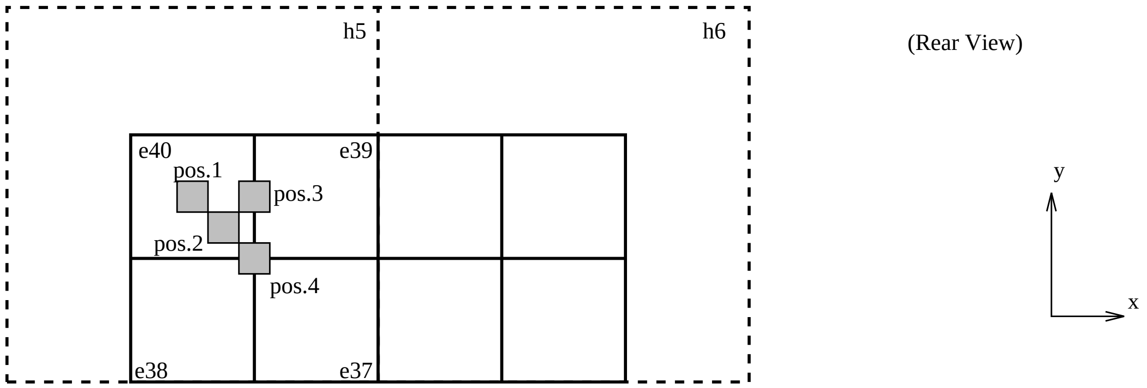

Figure 3: Schematic representation of the beam impact points. The solid (dashed) edges correspond to electromagnetic (hadronic) cells: h5 is the central hadronic cell of the 3×3 matrix and e40 is the corresponding electromagnetic cell centered on h5. The squares 1 (center), 2, 3 (border) and 4 (edge or corner) represent reference impact points for data taking.

Gain stability was monitored by injecting optical pulses from a flashlamp into the light mixer of each cell. The optical calibration events, available during standard data taking at a rate of ~ 1 Hz, allowed monitoring of short and long term gain variations which were compensated for offline. These gain variations turned out to lead to negligible corrections in the relevant cells. Also recorded in parallel were random triggers generated at a rate of $\sim$ 1 Hz by the data acquisition system for pedestal stability monitoring. Pedestals were found to be stable within 1.5 ADC counts throughout the test period.

Negatively charged beams of 1, 2, 3, 4, 5 and 7 GeV were sent into the detector at the impact points shown in Fig. 3. All data were recorded in mixed beam mode, i.e. without any trigger requirement on the type of incoming particle. The electron and pion samples have been defined offline, by cutting on the pulse amplitudes of the two Čerenkov counters in the beam line. Pile-up of beam events is minimized offline in two different ways:

- *early* pile-up is rejected by looking for any DSP channels significantly below the pedestal level. This can happen when SPACAL signals from a triggering event are sitting on the undershoot (i.e. the return to the baseline for a bipolar signal) of an immediately preceding event that did not fire the trigger coincidence (because it was out of the scintillator acceptance, for instance).

- *late* pile-up is rejected by looking for hits in the CAMAC TDC channel associated with the veto counter. This allows removal of events contaminated by late arrivals within the veto acceptance over a time window of about 200 ns.

The final pile-up contamination of the data samples is evaluated by comparing the effects of the global (*early* and *late*) pile-up cut on different regions of the electromagnetic energy spectra. Further reduction of pile-up is obtained by selecting only the tracks that are well reconstructed in the upstream drift chamber, yielding a final contamination between 1 and 3 % depending on the beam intensity. The effect of the pile-up rejection on the energy spectrum can be seen in Fig. 4 for a 2 GeV mixed beam.

3.2 Monte Carlo simulation tools

The SPACAL prototype tested at the CERN PS was simulated using the *fast* version of the H1 simulation program H1SIM [11]. In this *fast* simulation mode, the SPACAL medium is represented as a homogeneous mixture of lead and scintillator except at boundaries between supermodules where all the mechanical details are taken into account. The detector configuration used at CERN was simulated, with 64 electromagnetic cells, grouped in 4 supermodules, and 9 hadronic cells. A beam of dimension 1×1 cm^2 (as defined by the effective acceptance of the scintillators) containing a mixture of π^- and e$^-$ with energies ranging from 1 to 7 GeV was simulated.

The shower evolution of electromagnetic particles (e^- and γ) is fully parametrized [12] in the simulation when expected to be contained in the homogeneous medium. For hadrons (π, n, p) the situation is more complex since a lot of processes are involved and, in this case, hadrons are tracked by the GEANT [13] program through the SPACAL. Inelastic interactions and their products at each step of the hadronic shower evolution are determined via the GHEISHA [14] interface. Neutral pions decay into two photons and their energy deposition is parametrized in the same way as for electromagnetic showers.

The CERN PS test data presented in this paper were used as a basis for the tuning of the *fast* simulation program to reproduce the global energy response characteristics of the

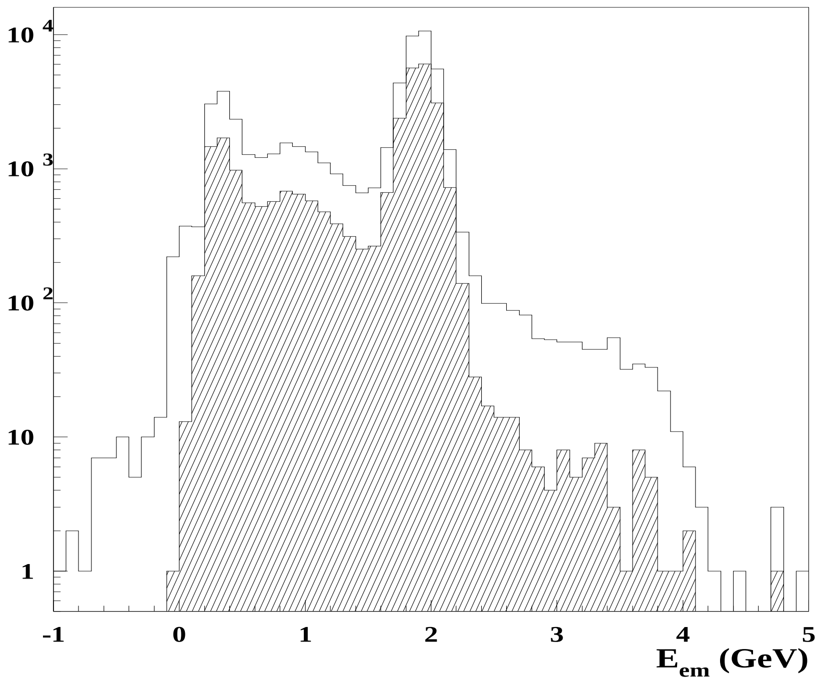

Figure 4: Energy distribution in the electromagnetic section for a 2 GeV mixed (electrons and pions) beam before (open histogram) and after (hatched histogram) the pile-up rejection.

SPACAL electromagnetic and hadronic calorimeter, using the same set of free parameters as for the tuning in the H1 LAr calorimeter [15]. The tunable parameters only play a role in the conversion of the various shower components to visible energy. These are the sampling fraction of minimum ionizing particles, the ratios of sampling fractions of electrons and hadrons to minimum ionizing particles and the sampling fluctuations for electromagnetic and hadronic showers. The main hadronic shower fluctuations are left to the detailed GEANT tracking and GHEISHA interactions.

In order to better reproduce the observed detector response, electronic noise as measured from random events is added to each Monte Carlo event on a cell by cell basis.

4 Electromagnetic and hadronic energy response

The energy, E_{em}, of the showers induced in the electromagnetic section is measured here by the following algorithm: a box of 5×5 cells is formed around the most energetic electromagnetic cell and the energy deposits of all the cells in this box are summed to obtain the total measured energy E_{em}. This box would correspond, in the H1 experiment, to a cone of about 3.5° half-opening, centered at the H1 interaction vertex. For the hadronic section, the definition of the clustering cone is extended to the whole sensitive volume, i.e. a box of 3×3 cells. The energy measured in the hadronic section is given by E_{had} and the total energy by $E_{em+had} \equiv E_{em} + E_{had}$. [1]

4.1 Response to minimum ionizing particles

The response to muons or punch-through (non-interacting) pions has also been studied from the CERN PS data. In absence of a refined offline muon tagging, pion data have been used: in order to minimize the sensitivity to inelastic interactions, the most probable value (mop) of the punch-through energy distribution is taken as the mip response.

In Fig. 5 the response of the electromagnetic section of the calorimeter to mips is presented as a function of the impact point of a 4 GeV π^- beam.

It is clear from the CERN PS test measurements that the fibre bundle region of 8 cm length, located behind each cell and collecting the light to the photocathode, has a strong influence on the mip response. The signal of a mip varies, as a function of the impact point, by up to 50 % from its minimal value. The oscillation of the response from cell to cell is well reproduced by the Monte Carlo simulation.

A correct measurement of the response to mips allows a determination of the so-called e/mip ratio, which relates the signals from electromagnetic showers to those from mips [17]. By comparing the mip response from the data (after correcting for bundle effects) to the response predicted by a detailed simulation of the SPACAL a ratio $e/mip = 0.87 \pm 0.03$ is found for the electromagnetic section. In the hadronic section the amount of noise (see section 6.1) in the readout affects the mip measurement in such a way that the corresponding e/mip ratio can't be precisely determined.

[1]Throughout the text, the subscript or superscript *em* and *had* will designate a quantity derived using information from only electromagnetic or only hadronic section respectively.

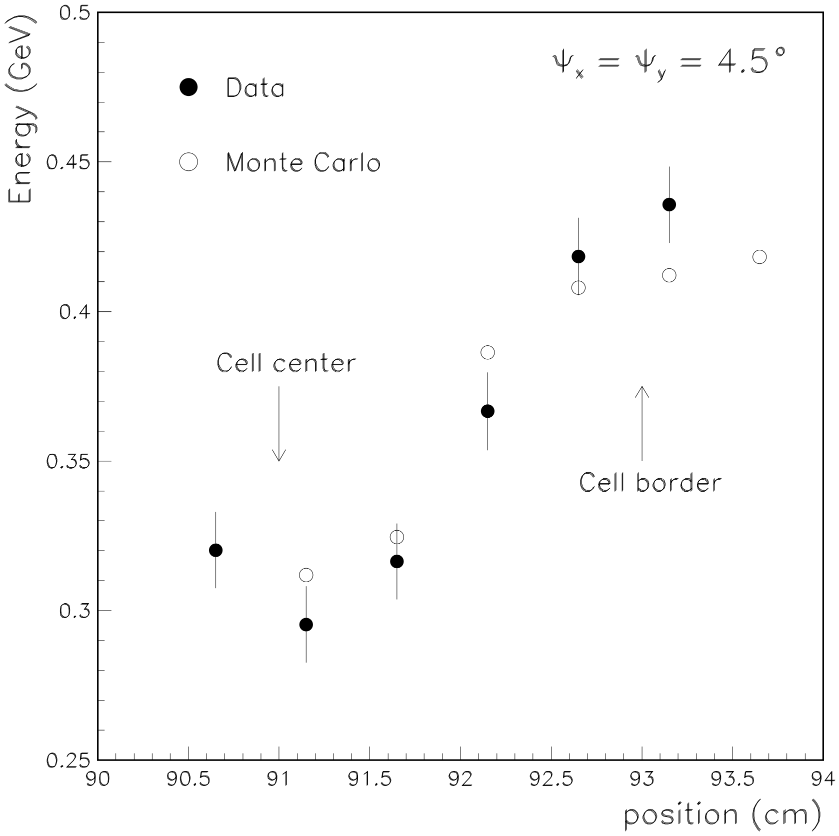

Figure 5: A diagonal scan over one electromagnetic cell showing a comparison between data and Monte Carlo of the energy response to mips (4 GeV pions). The variation of this response with the impact position, caused by the fibre bundle, is maximum at the cell border due to the incident angle $\psi_x = \psi_y \sim 4.5°$.

4.2 Resolution and linearity for electromagnetic showers

The performance of the SPACAL calorimeter in response to electromagnetic showers, as studied at CERN SPS and DESY test beams, are presented elsewhere [3]. At the CERN PS the linearity of the response, defined as the deviation of the measured energy from a straight line fit to the response curve, is maintained below 1 % between 1 and 7 GeV.

The energy resolution σ_E/E has been evaluated by fitting the data with a function including a sampling term $(1/\sqrt{E})$ and a constant term added in quadrature. The data considered for the fit were taken with the beam impinging on the center of an electromagnetic cell. The fit to the CERN PS data yields a sampling term of (7.6 ± 0.2) $\%/\sqrt{E}$ and a constant term of the order of (1.2 ± 0.3) %, compatible with the value presented in [3]. This corresponds to an energy resolution below 3 % at 7 GeV.

For the hadronic section, the test measurements at the CERN PS give an energy resolution of 10 % at 2 GeV compatible with (12.5 ± 3.0) $\%/\sqrt{E}$ + (3.8 ± 2.2) % obtained at the ITEP Proton Synchrotron [16]. As expected [17], the electromagnetic and hadronic resolution, σ_{em} and σ_{had}, follow the scaling given by:

$$\frac{\sigma_{had}}{\sigma_{em}} \propto \sqrt{\frac{d^{had}}{d^{em}} \frac{f^{em}_{mip}}{f^{had}_{mip}}} = 1.88 \pm 0.02$$

where d^{em} (0.5 mm) and d^{had} (1.0 mm) are the fibre diameters and f^{em} and f^{had} the sampling fractions for mips in each section (without bundle). The latter, defined as the ratio between the most probable values of the measured (visible) energy and the total deposited energy, are calculated from the detailed version of the SPACAL simulation. This gives $f^{em}_{mip} = (5.52 \pm 0.03)$ % and $f^{had}_{mip} = (3.07 \pm 0.03)$ %. The sampling fraction for electromagnetic showers f_e can be obtained by combining the mip sampling fraction with the e/mip ratio. This yields, for the electromagnetic section, $f^{em}_e = (4.80 \pm 0.02)$ %, consistent, at the 10 % level, with the value $f^{em}_e = 4.4$ % obtained via a detailed EGS simulation [18].

4.3 Response to interacting pions

The response of the electromagnetic and hadronic sections to interacting pions has been studied in detail at the CERN PS. Fig. 6 shows the energy distribution of 4 GeV pions in the two SPACAL sections with a comparison between data and Monte Carlo. The combined electromagnetic and hadronic response for interacting pions only is also shown in the same figure.

The total energy response in each section E_{em} (restricted to the cluster of 5 $\times$ 5 cells in the electromagnetic section) and E_{had} (extended to the whole hadronic section) was fitted to the sum of Landau and Gaussian distributions (see Fig. 7a and Fig. 8a).

The Landau distribution was selected to reproduce the response of non-interacting pions. Pions interacting inelastically are defined as those having the response described by the Gaussian distribution. The study was restricted to beam energies ≥ 2 GeV (3 GeV) when investigating the response of the electromagnetic (hadronic) section in order to allow the clearest separation possible between mips and interacting pions in the measured energy distributions.

4.3.1 Response of the electromagnetic section

Fig. 7a presents the distribution of E_{em} for 4 GeV incident pions together with the result of the fit. Given the depth of the electromagnetic section, about 63 % of the incident π^- are expected to interact inelastically in it: a detailed study using GHEISHA gives 65 % at 1 GeV, decreasing to 56 % at 7 GeV.

In Figs. 7b and 7c, the mean measured energy $\langle E \rangle$ and the energy resolution $\sigma_G/\langle E \rangle$ obtained from the Gaussian part of the fit for pions interacting in the electromagnetic section are shown as a function of the incident beam energy E_{beam}. The results are shown separately for different impact positions: the center, the border and the edge of an electromagnetic cell (see Fig. 3).

Fig. 7b shows a remarkable scaling of $\langle E \rangle$ with E_{beam}. Independent linear fits for the three impact point sets give slopes compatible within statistical errors and corresponding

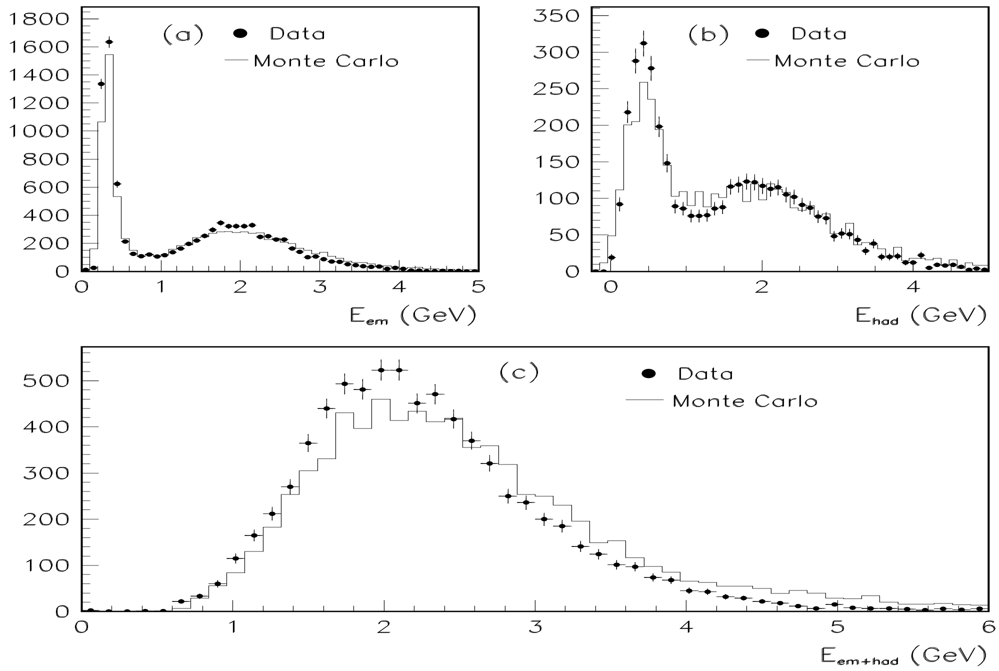

Figure 6: Energy distribution of 4 GeV pions (a) in the electromagnetic section, (b) in the hadronic section, (c) when interacting either in the electromagnetic or in the hadronic section. The data (points) are compared to the Monte Carlo (full lines).

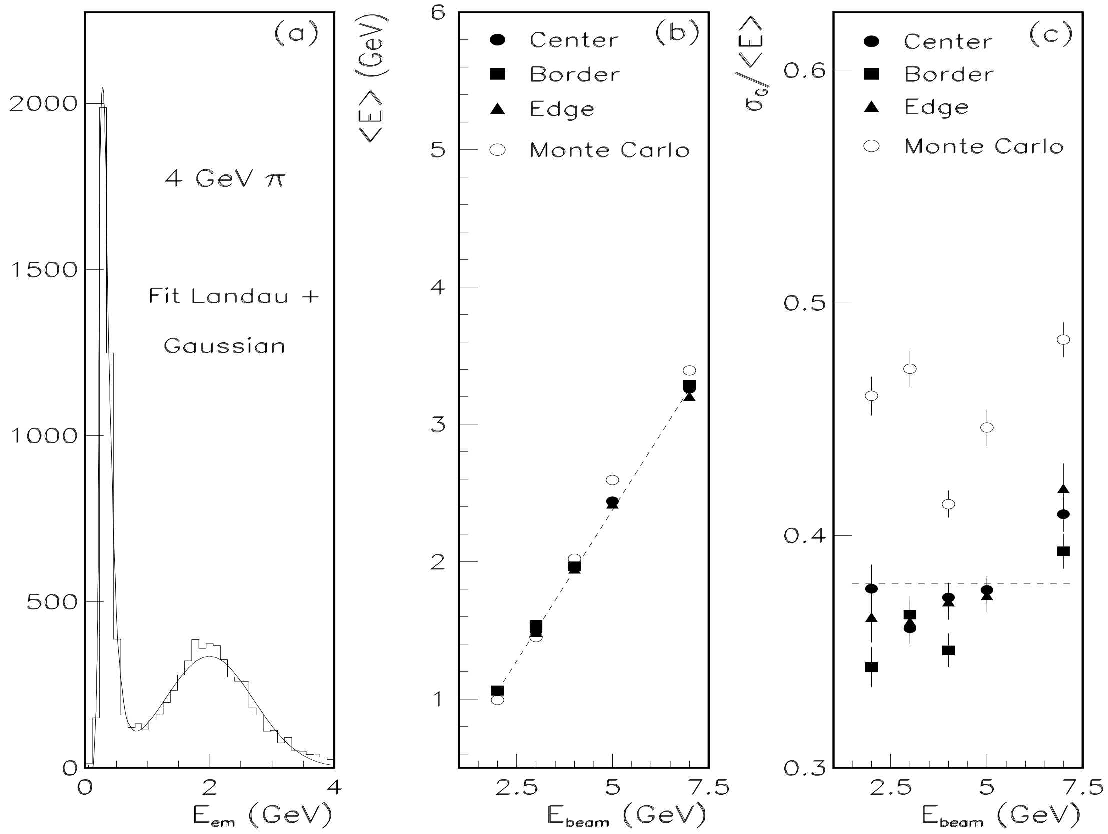

Figure 7: Response to pions interacting in the electromagnetic section: (a) example of typical fit to the energy response distribution E_{em}, (b) mean measured energy $\langle E \rangle$ and (c) fractional resolution $\sigma_G/\langle E \rangle$ as a function of the incident beam energy E_{beam}. The two last results are shown for three different impact positions at the center (dots), the border (squares) and the edge (triangles) of an electromagnetic cell. The position-averaged results of the simulation are shown (open circles). Only statistical errors are shown.

to a measured (visible) energy of $(45 \pm 1)\ \% \times E_{beam} + E_{offset}$ where E_{offset}=(175 ± 18) MeV. The deviations from linearity in the 2 to 7 GeV beam energy range are less than to 2 % for all the selected impact points. The linearity of the response is well reproduced by Monte Carlo as shown by the open circles in Fig. 7b, which represent the position-averaged results of the simulation.

This linearity is particularly striking since only a small but varying fraction of the visible energy is expected to originate from electromagnetic components initiated by π^0's. Indeed, one would expect f_{π^0}, the mean fraction of the incident energy converted into π^0's in a hadron-nucleus inelastic interaction, to be somewhat below 33%. Using GHEISHA, this fraction has been found to reach a plateau of about 25 % for energies above $\mathcal{O}$(10 GeV). At smaller energies, f_{π^0} decreases since more and more energy is transferred to protons, neutrons and to hadronic resonances and since particle masses play an increasingly important role.

From GHEISHA, $f_{\pi^0} \simeq 23$ % has been found on average at the primary inelastic interaction in the electromagnetic section for $E_{beam} = 7$ GeV, where the average π^0 multiplicity is about 2.3. The fraction then decreases (almost linearly) to $f_{\pi^0} \simeq 8.5$ % at $E_{beam} = 1$ GeV. At this energy the average number of π^0's created at the primary interaction is 0.4. On average 5.7 to 11.5 particles that carry more than 1% of the nominal energy are created for E_{beam} between 1 to 7 GeV respectively. The secondaries that are not absorbed by the medium will mostly escape the limited clustering volume of $\mathcal{O}(1\lambda_I)$ without undergoing inelastic interactions and eventual secondary interactions will not increase the π^0 component in a significant way.

Despite the fact that f_{π^0} increases as E_{beam}, the linearity of the energy response is maintained because of the energy leaking out of the calorimeter. There can be, in principle, two kinds of leakage: transversal and longitudinal. No significant transversal leakage, out of a cluster volume of 5×5 cells within the electromagnetic section, is observed in the CERN data. This can be studied by varying the transversal size of the clustering volume: the fraction of the measured energy contained in a volume of a given size approaches 100 % for a box of 5×5 cells in the 2 to 7 GeV range, demonstrating that any leakage on the sides can be neglected.

On the other hand, from GHEISHA, the longitudinal energy leakage for a π^- interacting in the electromagnetic section has been found to be on average 0.5 % at $E_{beam} = 1$ GeV, 12 % at $E_{beam} = 4$ GeV and 16 % at $E_{beam} = 7$ GeV. Since the mean energy transmitted to the secondaries at the primary interaction grows faster than their mean multiplicity, they become harder with increasing incident energy. Hence, the observed approximate scaling is explained by the fact that the increase of the fraction f_{π^0} is balanced by the increase of the longitudinal leakage as a function of E_{beam}. The bulk of the deposited energy turns out to be mainly associated with purely hadronic components.

The event-by-event fluctuations of the response are dominated by the energy sharing among particles emerging from the primary inelastic interaction. This leads to an energy resolution $\sigma_G/\langle E\rangle = (36 \pm 4)\,\%$ for pions interacting in the first λ_I. As it can be seen in Fig. 7c, there is an approximately *linear* scaling with the incident energy. The linear scaling and the mean fraction of visible energy are reproduced by the Monte Carlo, however the predicted resolution is slightly larger than the experiment.

4.3.2 Response of the hadronic section

As for the electromagnetic section, it is interesting to study the response of the hadronic section when forced to act as a first λ_I. To investigate this, the above analysis has been repeated but for π's having their first interaction in the hadronic section: a signal of less than 500 MeV compatible with a mip was explicitly required in the electromagnetic section.

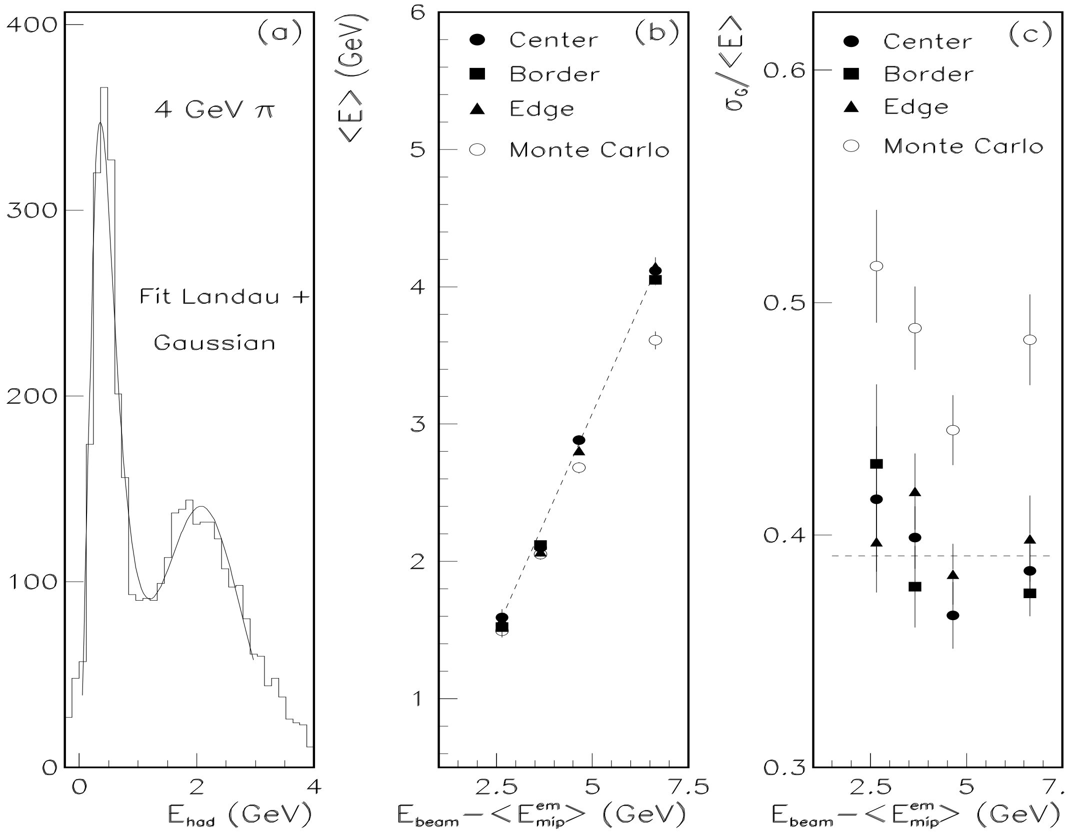

Figure 8: Response to pions interacting exclusively in the hadronic section: (a) example of typical fit to the energy response distribution E_{had}, (b) mean measured energy $\langle E \rangle$ and (c) fractional resolution $\sigma_G/\langle E \rangle$ as a function of the incident energy $E_{beam} - \langle E^{em}_{mip} \rangle$ where $\langle E^{em}_{mip} \rangle \sim 350$ MeV. The two last results are shown for three different impact positions at the center (dots), the border (squares) and the edge (triangles) of an electromagnetic cell. The position-averaged results of the simulation are shown (open circles). Only statistical errors are shown.

Fig. 8a presents the distribution of E_{had} for 4 GeV incident π^- and the result of the fit to the sum of a Landau and a Gaussian distribution. In Figs. 8b and 8c, the mean measured energy $\langle E \rangle$ and the resolution $\sigma_G/\langle E \rangle$ of the energy response obtained from the

Gaussian part of the fit for pions interacting exclusively in the hadronic section are shown as function of the incident energy $E_{inc} = E_{beam} - \langle E_{mip}^{em} \rangle$. Here $\langle E_{mip}^{em} \rangle \sim 350$ MeV is the mean energy lost by a mip in the electromagnetic section. The results are again shown separately for the different impact positions.

Here again, a remarkable scaling of $\langle E \rangle$ with E_{inc} is found (Fig. 8b). A mean measured (visible) energy of $(65 \pm 3)\,\% \times E_{inc} - E_{offset}$ where $E_{offset} = (225 \pm 16)$ MeV is observed (compatible within errors for the three sets of impact points) in a volume of 3×3 cells which is transversely 3.2 times larger than the one used in the electromagnetic section. The deviations from linearity in the 3 to 7 GeV range are less than 5% for the various impact points. The linearity of the response is well reproduced by Monte Carlo as it is shown by the open circles in Fig. 8b, again representing the position-averaged results of the simulation.

As in the case of the electromagnetic section, the linear scaling of the energy response as a function of the incident energy is due to the balance between f_{π^0} and the longitudinal leakage. In the hadronic section, since the same inelastic interaction π-Pb is involved at the very first interaction, the fraction f_{π^0} is the same as for the electromagnetic section. From GHEISHA, the longitudinal leakage has been measured to be negligible for an incident energy E_{beam} of 1 GeV, 7 % at $E_{beam} = 4$ GeV and 15 % at $E_{beam} = 7$ GeV. Also, when subtracting the estimated f_{π^0} from the mean deposited energy, the response to the purely hadronic components of the shower in the hadronic section turns out to be about 40 to 50 % higher than in the electromagnetic section.

The energy resolution, $\sigma_G/\langle E \rangle = (39 \pm 4)\,\%$, scales *linearly* with the incident energy (Fig. 8c). This value is only slightly larger than the one obtained in the electromagnetic section. This is despite the fact that the sampling fraction (for electromagnetic showers or mips) is about twice as small in the hadronic section, which indicates that here again the resolution is dominated by the fluctuations at the primary inelastic interaction. The linear scaling and the mean fraction of visible energy are reasonably well reproduced by Monte Carlo but, once again, with a slightly larger resolution.

4.3.3 Combined response of electromagnetic and hadronic sections

Fig. 9a presents the distribution of E_{em+had}, the sum of the electromagnetic E_{em} and hadronic E_{had} energies, for 4 GeV incident π^- interacting at least in one of the two sections. The asymmetric shape of the distribution would be best fitted by a Landau function: however, in order to be consistent with the results presented for E_{em} and E_{had} separately, we fit the central part of the E_{em+had} spectrum to a Gaussian function.

In Figs. 9b and 9c, the mean measured energy $\langle E \rangle$ and the resolution $\sigma_G/\langle E \rangle$ obtained from the Gaussian fit for pions interacting in any of the calorimeter sections are shown as function of E_{beam}.

As it can be seen from Fig. 9c, combining the response from the two sections improves the energy resolution which is found to be $\sigma_G/\langle E \rangle = (29 \pm 2)\,\%$. Of course, one must bear in mind that the effectiveness of such an improvement is somehow limited by the non-Gaussian tails as shown in Fig. 9a for the 4 GeV case.

Combining linearly E_{em} and E_{had} with different scale factors and minimizing the dispersion relative to the incident energy, an optimal constant scale factor of ~ 1.94 is found

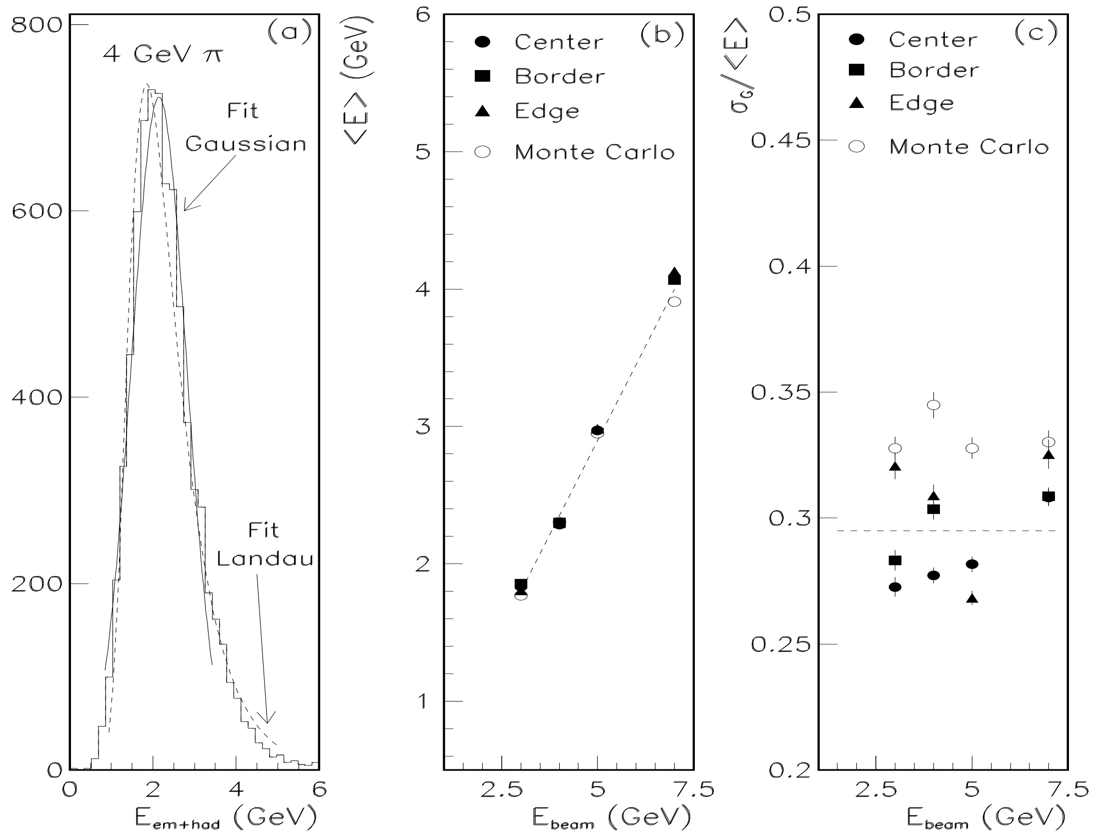

Figure 9: Response to pions interacting either in the electromagnetic or in the hadronic sections: (a) examples of typical Gaussian and Landau fits to the energy response distribution E_{em+had}, (b) mean measured energy $\langle E \rangle$ and (c) fractional resolution $\sigma_G/\langle E \rangle$ extracted from the Gaussian fit as a function of the incident beam energy E_{beam}. The two last results are shown for three different impact positions at the center (dots), the border (squares) and the edge (triangles) of an electromagnetic cell. The position-averaged results of the simulation are also shown (open circles). Only statistical errors are shown.

for the signal in the electromagnetic section. The corresponding result for the hadronic section varies from ~ 1.29 at 3 GeV to ~ 1.46 at 7 GeV. However the introduction of such scale factors does not significantly improve the energy resolution for the combined response because of the non-Gaussian tails mentioned above. Of course, the development of a complete technique of weighting [19] of the hadronic energy deposited in the two sections of the SPACAL calorimeter for the hadron shower energy reconstruction within the H1 environment would need a detailed study which goes beyond the topic of this paper.

5 Shower profiles

5.1 Lateral profiles

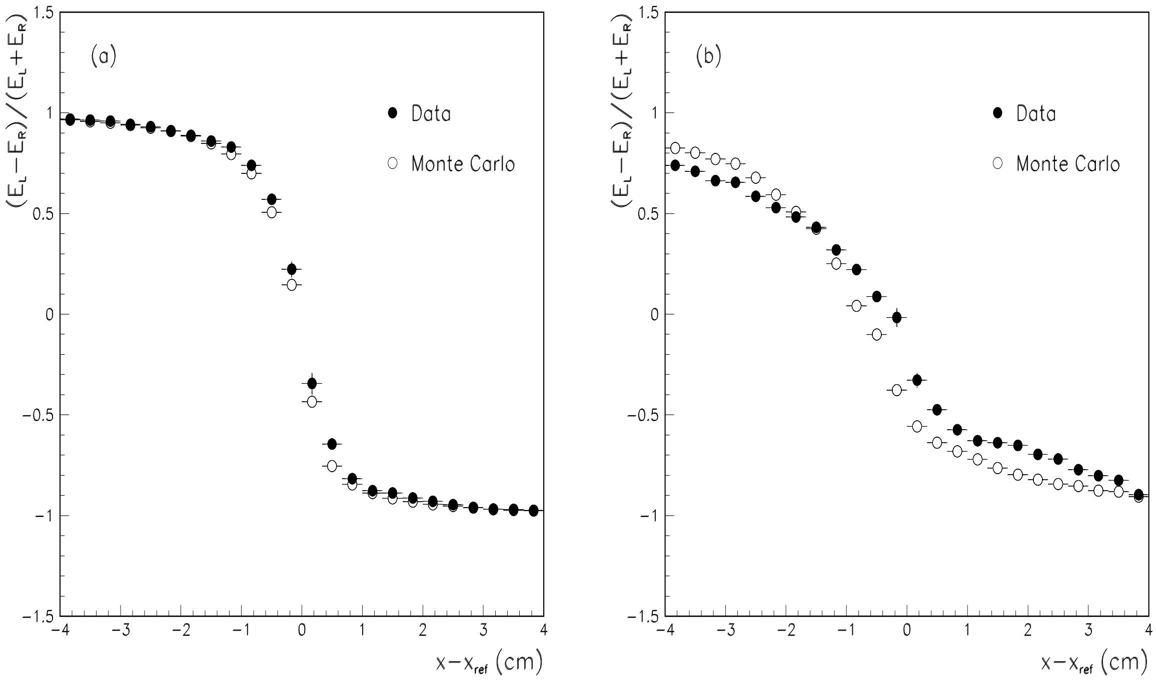

Figure 10: Energy sharing $(E_L - E_R)/(E_L + E_R)$ on the two sides of a reference plane for an incident beam energy of 4 GeV for (a) electrons and (b) interacting pions.

Fig. 10 presents the sharing between the energy deposited in the electromagnetic section on the left (E_L) and on the right (E_R) side of a fixed reference plane when a position scan with 4 GeV electrons (Fig. 10a) and with 4 GeV interacting pions (Fig. 10b) is performed in the direction perpendicular to this reference plane. A comparison with the Monte Carlo simulations is presented on the same figure.

From such lateral profiles, the characteristic lateral dimension of the shower evolution can be extracted by assuming a radial function $f(r) = 2\pi r R(r)$, where $R(r)$ is the radial energy density, for the description of the transversal energy profile of the shower [20]. Three basic energy density functions $f(r)$ and their linear combinations have been considered [12]:

$$
\begin{aligned}
f_1(r) &= \frac{2rR_0^2}{(r^2+R_0^2)^2} \\
f_2(r) &= \frac{1}{R_0}e^{-r/R_0} \\
f_3(r) &= \frac{r}{R_0^2}e^{-r/R_0}
\end{aligned}
$$

A characteristic transversal scale, the radius $2 \times R_0$ corresponding to 95 % energy containment has been defined. The energy sharing $(E_L - E_R)/(E_L + E_R)$ distribution is then related to the integral of the radial function $f(r)$ over the radius $2 \times R_0$. By fitting the energy sharing distribution, R_0, left as a free parameter in the fitting procedure, is obtained. The typical lateral dimension $2 \times R_0$, which is directly related to the Molière radius R_M of the detector, is a mean value obtained from the results of the different fits of the sharing energy distribution using the three radial functions $f_i(r)$ and their linear combinations. The errors given are an indication of the spread of the results.

For 4 GeV electrons, R_0 has been evaluated as (2.1 $\pm$0.1) cm for the data and (2.1 $\pm$0.1) cm for Monte Carlo giving excellent agreement between data and simulation. For 4 GeV π's, the lateral dimension R_0 of the shower has been evaluated as (7.5 $\pm$0.5) cm for the data and (5.5 $\pm$0.5) cm for the Monte Carlo simulation: the slight discrepancy between data and Monte Carlo might suggest a non optimal treatment of the transverse energy spread in the inelastic interactions generated by GHEISHA.

Because of the small available statistics, the evolution of the lateral dimension of the shower in the electromagnetic section as a function of the beam energy could not be evaluated precisely. However, a general trend could be deduced. The lateral dimension of showers induced by electrons is more or less stable with the energy: this is in good agreement with the Monte Carlo. In the case of pions, the lateral dimension of the shower increases as a function of the energy. The Monte Carlo reproduces the same trend but with a lateral dimension smaller than that observed in the data.

5.2 Longitudinal properties

The energy sharing from interacting pions between the electromagnetic and the hadronic section is directly related to the properties of the calorimeter as well as to the energy of the incoming particles (especially below 10 GeV, where the interaction cross section of pions varies significantly with energy). A suitable variable for the study of the longitudinal energy sharing is the ratio R_E defined as

$$R_E = \frac{E_{em}}{E_{em} + E_{had}}$$

Fig. 11 shows how 4 GeV electrons and pions populate different parts of the E_{em} versus R_E plane: electrons leave all their energy in the electromagnetic section, thus giving a R_E distribution peaked at 1. Pions occupy a wider region of the plane, falling into different domains according to their behaviour in the two calorimeter sections.

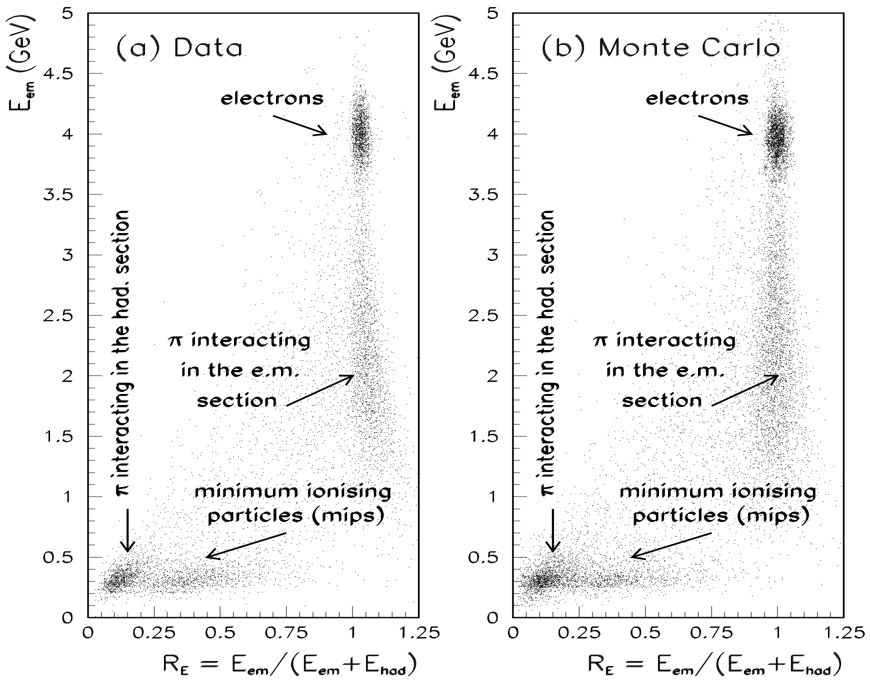

Figure 11: Distribution of the energy E_{em} deposits in the electromagnetic section as a function of the ratio $R_E = E_{em}/\left(E_{em} + E_{had}\right)$ for an incident beam energy of 4 GeV for (a) data and (b) Monte Carlo.

6 e/π separation

We present here the results of the experimental study on electron identification in the 2 to 7 GeV energy range based on e/π estimators that profit of the fine lateral segmentation of the electromagnetic section as well as of the $1\lambda_I$ longitudinal segmentation by the two sections of the calorimeter. Furthermore, a comparison is shown between these results and the Monte Carlo simulation.

6.1 Preliminary selection

In order to reject pions punching through the electromagnetic section, a cut on the energy deposit in the hadronic section can be applied: ideally one would be satisfied with a cut on the total hadronic energy set well below the mip level. However, data from the hadronic section have been affected during all the test period by a significant amount of mostly coherent noise ($\sigma_{noise} \simeq 6$ MeV/channel) and by gain and pedestal instabilities. This reduces the rejection power of any estimator based exclusively on the hadronic energy deposit.

The longitudinal energy sharing ratio R_E defined in section 5.2 turns out to be an optimal estimator for the rejection of mips (see Fig. 11) since they tend to accumulate in the low E_{em}, low R_E region and can thus be easily removed by a proper cut on R_E.

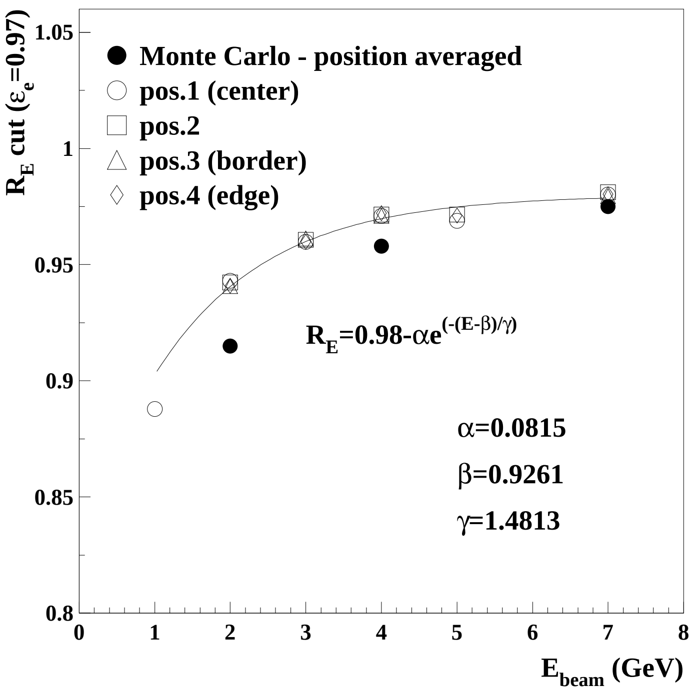

Figure 12: R_E cut giving 97% electron efficiency at different electron beam energies and impact points. The curve is the result of a fit to the data points. The position-averaged results of the simulation are shown.

Fig. 12 shows, for different beam energies and impact points, the cut that has to be imposed on R_E in order to accept 97 % of the incoming electrons. Such a cut can be easily parametrized as a function of the electron energy, independent of the impact point. Due to the high noise in the hadronic section, the cut on R_E increases with the energy of the incoming electrons.

The effect of the R_E cut on the pion energy distribution in the electromagnetic section can be seen in Figs. 13a and 13b where the same quantity is plotted before (open histograms) and after (hatched histograms) the selection, for pions of 2 and 5 GeV respectively.

The *rejection factor* $R_{e/\pi}$ has been defined as the ratio ϵ_e/ϵ_π of the electron detection efficiency divided by the probability to misidentify a pion as an electron. Fig. 14 shows

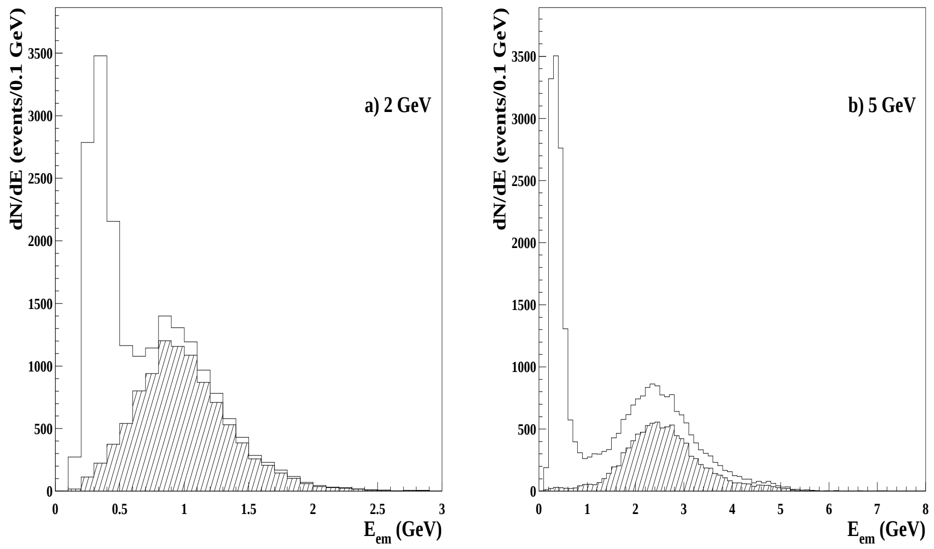

Figure 13: E_{em} for 2 GeV (a) and 5 GeV (b) negative pions, before (open) and after (hatched) the R_E selection.

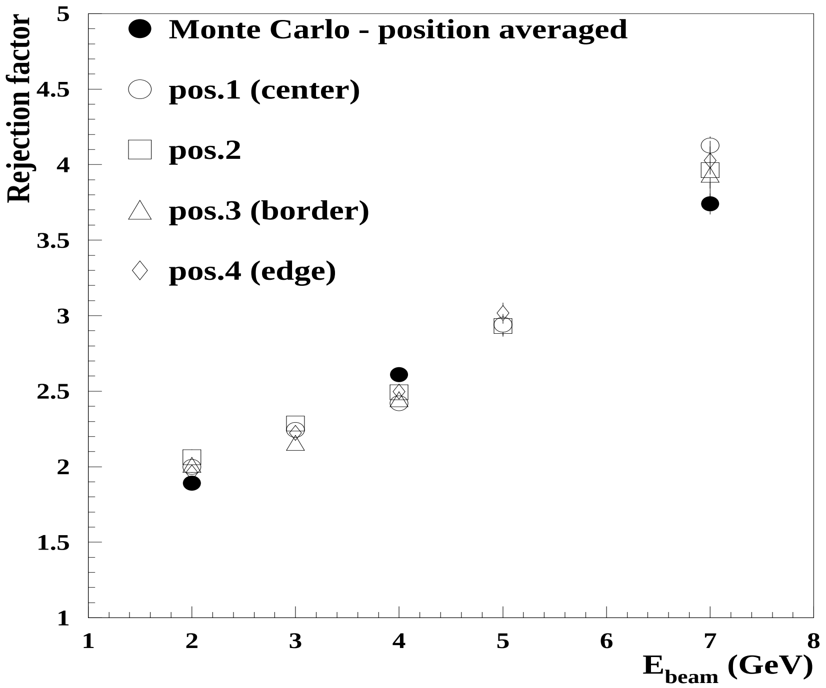

Figure 14: e/π rejection factor of the R_E selection for (97$\pm$2) % electron efficiency as a function of the pion nominal energy. The position-averaged results of the simulation are shown.

the rejection factor $R_{e/\pi}$ of the R_E selection for the analyzed beam energies and impact points, for an electron efficiency of (97±2) %. Monte Carlo position-averaged predictions are also shown in the picture.

6.2 Shower estimators

Once an efficient and reliable way of rejecting punch-through pions has been defined, shower estimators that reject the remaining pions on the basis of the shower shape in the electromagnetic section alone can be developed. Shower moments turn out to be well suited to this task. In particular, the second moment, which essentially measures the lateral spread of the shower, shows the best performance in terms of e/π separation and can be used on a standalone basis (i.e. with no information coming from other detectors than the SPACAL). Such a feature, as already mentioned, is important if a fast electron identification is to be achieved in H1.

6.2.1 Shower moments

Shower properties can be parametrized in terms of the *moments* of their energy distribution around the impact point. The k-th (central) moment of the shower along the x axis has been defined as [2]:

$$\mu_k = \left(\frac{\sum_i w_{ik} \left(x_i - \bar{x} \right)^k}{\sum_i w_{ik}} \right)^{1/k}$$

where x_i is the coordinate of the i-th cell and $\bar{x}$ is the coordinate of the particle impact point. The definition is such that moments of any order have the dimension of a length. For k=2 (lateral spread), the latter can be approximated by the shower center of gravity (c.o.g.):

$$\bar{x} = \frac{\sum_i w_{i1} x_i}{\sum_i w_{i1}}$$

6.2.2 Determination of the weights

The weights w_{ik} are directly related to the energy deposited in the calorimeter cells. However, a simple linear energy weighting (w_{ik}=E_i) leads to a strong position dependence of the shower moments (for instance the well known *S-curve* for the shower c.o.g. [21]). Such a dependence can be, in principle, corrected for, but the parametrization may have to take into account several factors (like the energy and the incidence angle of the incoming particle), thus becoming complicated. A simpler solution [21] is to define the weights w_{ik} as:

$$w_{ik} = max \left\{ 0, W_{0,k} + \ln \frac{E_i}{E_{tot}} \right\}$$

[2]Of course, the same definition holds for the y coordinate.

where E_i is the energy deposited in the i-th cell, E_{tot} is the total energy of the shower and $W_{0,k}$ is a free parameter.

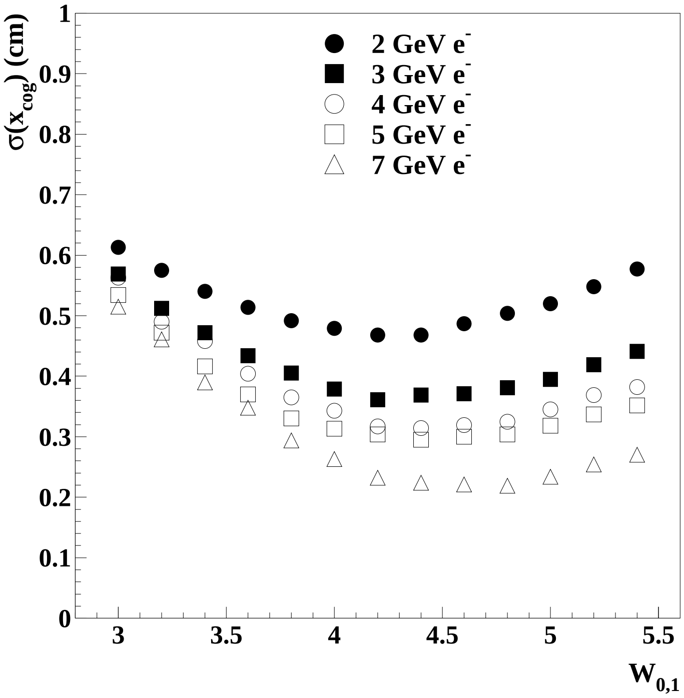

Figure 15: Resolution of the x coordinate of the shower c.o.g. as a function of the parameter $W_{0,1}$.

Fig. 15 shows how the resolution of the shower c.o.g. is affected by the choice of the cut $W_{0,1}$ used in the calculation of the logarithmic weights. Data from different impact points at a given energy are merged. The energy dependence for the minimum of $\sigma(\mu_{1x})$ being negligible, $W_{0,1}$ has been fixed at a value of 4.4.

The logarithmic cut $W_{0,k}$ has to be tuned separately for each order of shower moments. The effect of different choices of $W_{0,2}$ on μ_{2x} is shown, for a 4 GeV beam, in Fig. 16.

Lower $W_{0,2}$ values improve the e/π separation for impact points around the centre of a cell but introduce a strong dependence of the separation itself on the impact point. Once again, one must choose between an ad hoc parametrization for μ_{2x} (i.e. one that takes into account, in the definition of $W_{0,2}$, the dependence from the impact point, the angle and the energy of the incident particle) and a definition that cancels, as much as possible, all dependences.

Following the latter strategy, the choice of $W_{0,2}$ has been optimized by maximizing a position-averaged e/π resolving power defined as:

$$R(E_e) = \frac{\left(\bar{\mu}_{2,\pi} - \bar{\mu}_{2,e}(E_e)\right)^2}{\sigma_{\mu_\pi}\sigma_{\mu_e}(E_e)}$$

where $\bar{\mu}_{2,e}(E_e)$ is the mean value of the second moment distribution for electrons of energy

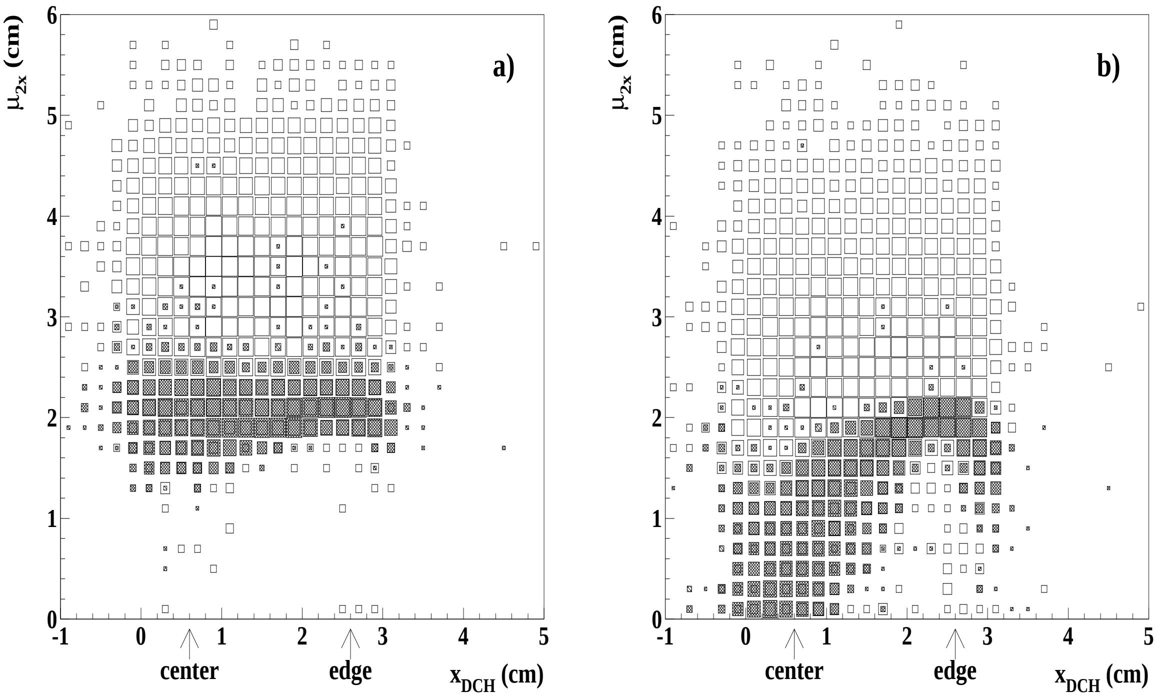

Figure 16: Second moment (x coordinate) vs. reconstructed impact point (as given by tracking) for two different values of $W_{0,2}$: a) $W_{0,2}$=4.85, b) $W_{0,2}$=3.5; electrons are represented by the filled boxes, pions by the open ones.

E_e and $\sigma_{\mu_e}(E_e)$ is its dispersion; $\bar{\mu}_{2,\pi}$ and σ_{μ_π} are the equivalent quantities for pions of incident energies integrated between 2 and 7 GeV.

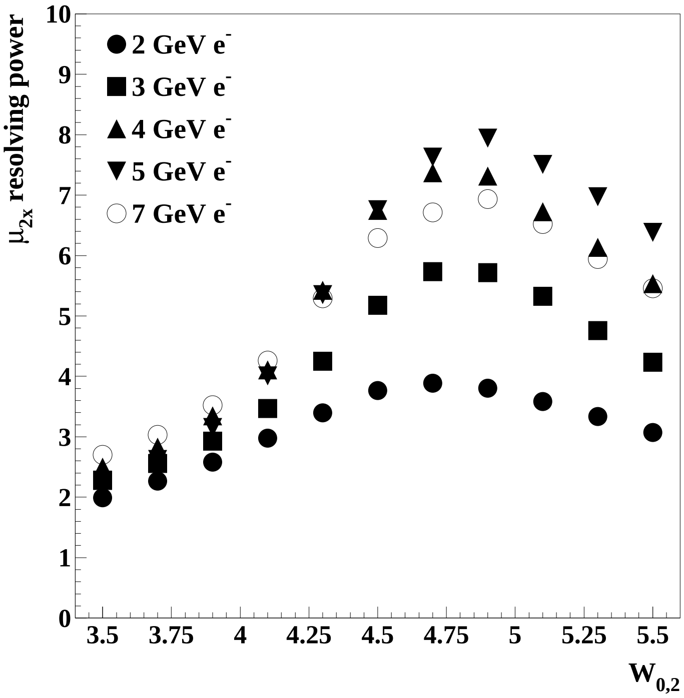

Figure 17: μ_2 resolving power $R(E_e)$ versus $W_{0,2}$, x coordinate.

In Fig. 17, $R(E_e)$ is shown as a function of the logarithmic cut $W_{0,2}$ for x coordinates (y coordinates show the same behaviour). $R(E_e)$ has a maximum around $W_{0,2} = 4.85$, with no significant energy dependence. This value has been used throughout the rest of the analysis. The dependence of the second moment on the choice of the cut parameter $W_{0,2}$ is well reproduced by the simulation (see Fig. 18).

6.3 Pion rejection factors

Pion rejection factors have been studied for the quadratic combination of the x and y components of the shower second moment:

$$\mu_2 = \sqrt{\mu_{2x}^2 + \mu_{2y}^2}$$

the two components being uncorrelated.

The cut on μ_2 has been parametrized as a function of the energy deposit in the electromagnetic section, with the purpose of keeping the electron efficiency at 90%. Fig. 18 shows the μ_2 cut values for electrons at different energies and impact points, together with the resulting fitted function and with the position-averaged Monte Carlo prediction which well reproduces the data. The systematic error introduced by this parametrization on the final rejection factors is of the order of 3 %.

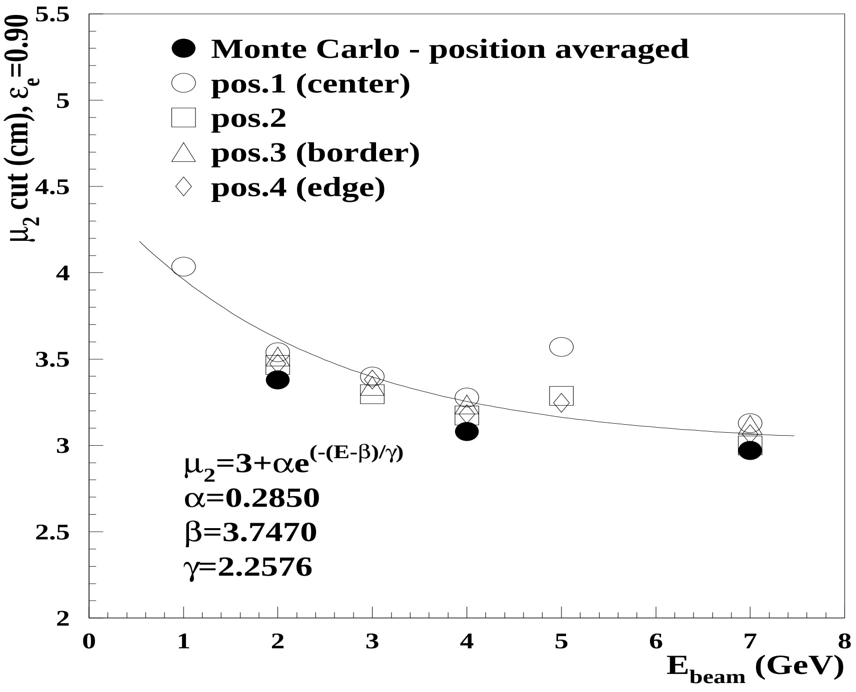

Figure 18: 90% efficiency cuts on μ_2 as a function of the energy of the incoming electron, for different impact points. The position-averaged results of the simulation are shown (black circles).

Fig. 19 shows the energy deposited by pions in the electromagnetic section before and after the e/π separation procedure, for incident energies of 4 and 7 GeV; the accumulation at E_{em} values around the incident pion energy can't be explained by electrons contaminating the pion sample (the combined inefficieny of the two Čerenkov counters used to tag electrons being much smaller than 0.1 %). The number of events is consistent with the expected number of fully contained charge exchange interactions between the incoming pions and the protons of the detector medium [7, 22].

Fig. 20 shows the rejection factors obtained at different impact points as a function of the incident pion energy, where a cutoff of 1 GeV on E_{em} has been imposed (the lowest accepted electron energy in H1 being well above that value). $R_{e/\pi}$ increases from about 20 for 2 GeV pions to about 250 for 7 GeV pions, corresponding to a probability of 5 % (0.4 %) that a pion of 2 (7) GeV fake an electron of more than 1 GeV. No significative dependence on the impact point has been observed, within the available statistics.

Besides this kind of rejection factors, which are integrated over all measured energies above a certain E_{em} value, it is important to evaluate the probability that a pion of a given incident energy can fake an electron in a well defined energy range. This probability,

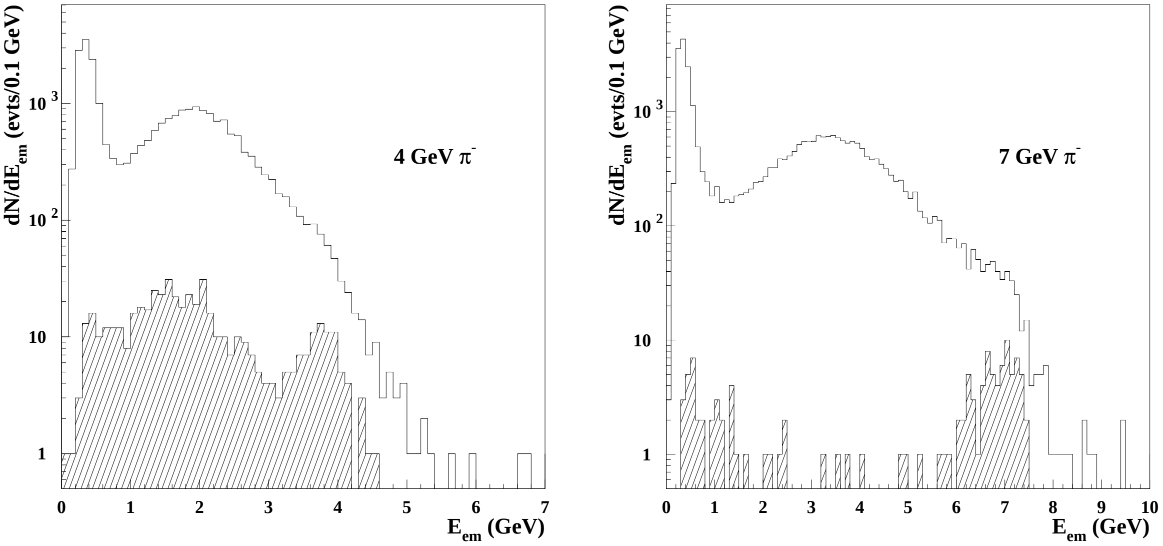

Figure 19: Energy spectra of 4 GeV π^- (left) and 7 GeV π^- (right) before (open) and after (hatched) the rejection procedure.

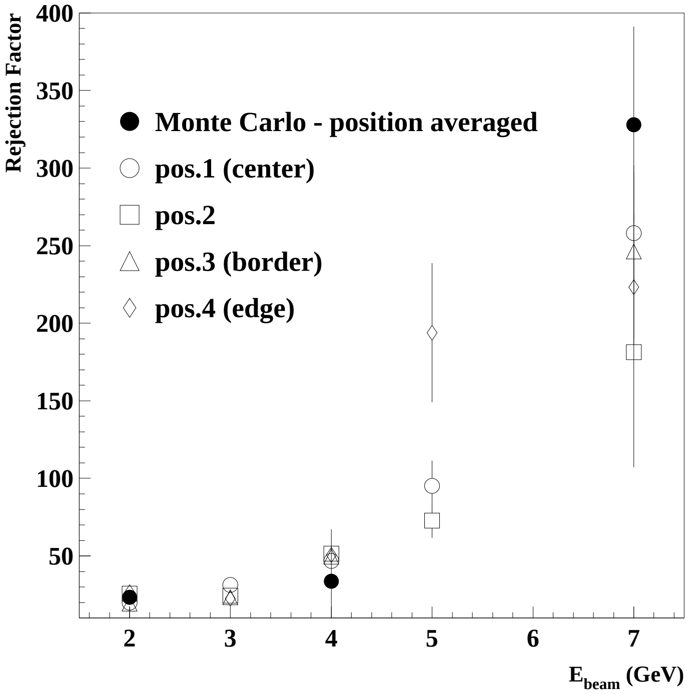

Figure 20: e/π rejection factors vs. pion incident energy at 90% efficiency for electrons. A cut at 1 GeV has been applied. The position-averaged results of the simulation are shown.

convoluted with the energy spectrum of pions produced in photoproduction events at HERA, yields the amount of background that contaminates the electron sample from DIS events at small x in H1. For each pion incident energy, the number of events that fake an electron of a given energy $E_{em} \pm 3\sigma_{em}(E_{em})$ is used to derive the corresponding differential rejection factor. Fig. 21 shows the obtained $R_{e/\pi}$ values for pions of 2 to 7 GeV incident energy as a function of E_{em}. For the evaluation of these differential factors the cutoff at 1 GeV has been removed.

As it can also be seen from Fig. 21, the number of 7 GeV pions that fake an electron in any E_{em} window in the 1 to 5 GeV range only allows to determine a lower limit for the corresponding rejection factors, due to the limited statistics: the data points for which only a lower limit could be calculated are marked with arrows on the picture. The obtained values span almost two orders of magnitude, ranging from 20 for 2 GeV pions faking 1 GeV electrons to more than 3000 for 7 GeV pions faking an electron of less than 6 GeV. This corresponds, in the first case, to a probability of 2.5 % for 2 GeV pions to be misidentified as 1 GeV electrons and, in the second case, to a probability less than 0.03 % for 7 GeV pions to be misidentified as an electron in any window opened below 6 GeV. The decrease of the rejection factors for E_{em} values approaching the pion incident energy is due, as mentioned above, to the fraction of charge exchange processes in which the produced π^0 is fully contained in the electromagnetic section. The probability for this kind of events sets an ultimate limit to the capability of separating electrons from pions on the basis of calorimetric information alone. At 3 GeV (7 GeV), 0.5 % (0.25 %) of the incoming pions are identified as electrons of the same energy. These probabilities are consistent with the predicted ratio between the charge exchange and the inelastic cross sections for pions in the energy range under study.

7 Conclusions

A detailed study of the response to electrons and hadrons for the H1 lead/fibre calorimeter has been made at the CERN PS. Two portions of the electromagnetic and hadronic section have been exposed to electron and pion beams in the 1 to 7 GeV energy range.

The response to mips and interacting pions has been examined and compared to Monte Carlo simulation. The measured energy of pions interacting either in the electromagnetic or in the hadronic section scales linearly with the incident energy, with a scaling factor of (45$\pm$1) % and (65$\pm$3) % respectively, and a corresponding energy resolution of (36$\pm$4) % and (39$\pm$4) %. The energy resolution for the combined energy response is found to be (29$\pm$2) %. The Monte Carlo simulation well describes the observed energy distributions in the two sections as well as their combined response.

Shower profiles of 4 GeV electrons and pions have been studied in detail: the transversal shower size (at 95% containment) has been measured to be (2.1$\pm$0.1) cm for electrons and (7.5$\pm$0.5) cm for pions, again with good agreement between real and simulated data.

The e/π separation capabilities of the SPACAL calorimeter have been analyzed. Estimators for an efficient e/π separation have been tuned, and applied to real and simulated events in the 2 to 7 GeV beam energy range. Typical e/π rejection factors range between 20 (for 2 GeV pions faking 1 GeV electrons) and about 860 (for 7 GeV pions faking 6 GeV

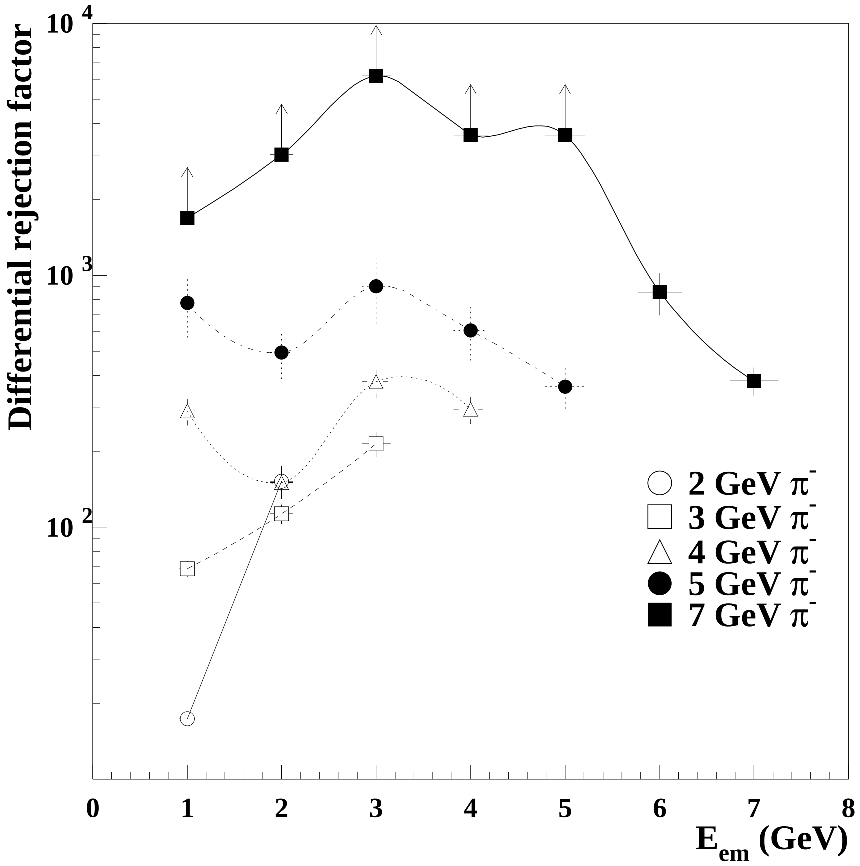

Figure 21: e/π rejection factors as a function of the energy deposited in the electromagnetic section, at 90% efficiency for electrons. Data points marked with arrows are lower limits for the corresponding rejection factors.

electrons). The probability for pions of any measured energy to be misidentified as 4 GeV electrons is 1/300 for an electron detection efficiency of 90 %. Energy integrated rejection factors are also derived and compared to Monte Carlo, with a satisfactory agreement. These results demonstrate the capability of the H1 SPACAL calorimeters to isolate DIS events from the hadronic photoproduction background even for energies of the scattered electron of the order of a few GeV, thus enhancing the sensitivity to the low x physics regime.

8 Acknowledgements

We wish to thank all the technical staff from the institutes participating to the H1 SPACAL project for their outstanding support. We are thankful to F. Brasse for his great committment in planning and starting the detector upgrade. We are also grateful to the CERN PS staff for the precious help we received during all the beam test periods.

References

[1] H1 Collaboration, *Technical Proposal to Upgrade the Backward Scattering Region of the H1 Detector*, PRC 93/02, March 8, 1993.

[2] H1 Collaboration, *The H1 Detector at HERA*, DESY 93-103.

[3] H1 SPACAL group, *Performance of an Electromagnetic Lead/Scintillating-Fibre Calorimeter for the H1 Detector*, DESY 95-165 (to be submitted to Nucl. Instr. and Meth.).

[4] K. Bätzner et al., *Secondary beams for tests in the PS East experimental area*, PS/PA Note 93-21.

[5] H. Deckers, Diploma Thesis, University of Dortmund, Germany, unpublished (1994)^{WWW}.

[6] H1 SPACAL group, *SPACAL Technical construction paper*, in preparation.

[7] M. Aguilar-Benitez et al., *Review of Particle Properties*, Phys. Rev. D (1994).

[8] J. Janoth, Diploma Thesis, University of Dortmund, Germany, unpublished (1993)^{WWW}.

[9] H1 SPACAL group, *SPACAL-H1: the New Lead/Scintillating-Fibre Upgrading the Backward Part of H1*, presented at HEP Conference at Brussels (Belgium).

[10] V. Boudry et al., *The Inclusive Electron Trigger for SPACAL: Design and CERN-Test Results*, H1 Internal Note 03/95-430.

[11] *A guide for the H1 simulation program H1SIM*, version 3.06/23, H1 Internal Note 03-11/89.

[12] G. Grindhammer, M. Rudowicz, S. Peters, SLAC-PUB-5072, August 1989.

[13] R. Brun et al., *GEANT User's Guide*, CERN DD/EE/84-1, 1987.

[14] H.C. Fesefeldt, Technical Report PYTHIA 85-02, Aachen, Germany, September 1985.

[15] *Performance of the H1 Liquid Argon Calorimeter*, presented at the 3rd International Conference in High Energy Physics, Corpus Christi, Texas (1992), and references therein.

[16] H1 SPACAL group, *H1 Backward Upgrade with SPACAL Calorimeter: Hadronic Section*, in preparation as DESY report.

[17] R. Wigmans, CERN-PPE/91-205;
M. Livan, V. Vercesi and R. Wigmans, CERN 95-02.

[18] M. Dirkmann, Diploma Thesis, University of Dortmund, Germany, unpublished (1995)^{WWW}.

[19] H1 Calorimeter group, *Study of Software Compensation for Single Particles and Jets in the H1 Calorimeter*, contributed paper to the XXV International Conference on High Energy Physics, Singapore, 1990.

[20] D. Acosta et al., Nucl. Instr. and Meth. A316 (1992) 184.

[21] T.C. Awes et al., Nucl. Instr. and Meth. A311 (1992), 130.

[22] G. Giacomelli et al., Phys. Rep. 23C (1992).

^{www} These documents can be found on the World Wide Web.
Address: http://dice2.desy.de/h1/www/h1det/calo/spacal/pubs.html